Plasmonic spectroscopy of 2D densely packed and layered metallic nanostructures

A. N. Ponyavina[1*] **and S. M. Kachan**[2]

[1] Institute of Physics, National Academy of Sciences of Belarus, Nezavisimosti Ave. 68, Minsk, 220072, Belarus

[2] Belarusian National Technical University, Khmelnitskogo Str. 9, Minsk, 220013, Belarus

Abstract. This chapter is an overview of size and concentration effects on electrodynamic coupling in two-dimensional densely packed arrays of metallic nanospheres in the frequency range of the surface plasmon resonance (SPR). Our theoretical analysis is based on the statistical theory of multiple scattering of waves. We show that concentration effects, such as the enhanced long-wavelength transmission of light and the strong resonance quenching of transmission, are effectively interpreted in terms of constructive and destructive interference of waves incident on and scattered by a monolayer of closely-packed submicrometer plasmonic particles. The concentration SPR red shift observed in the case of dipole metal nanoparticles is highly sensitive to the matrix refractive index and results from lateral near-field couplings. We also demonstrate phenomena caused by a strong plasmonic–photonic confinement in multilayered metal–dielectric nanostructures consisting of densely packed monolayers. For example, we show that employing the size and/or concentration gradient of dipole metallic nanoparticles in a quarter-wavelength multilayered system allows one to achieve an almost total absorbance.

Keywords: metallic nanostructures, surface plasmon resonance, electrodynamic coupling

1. Introduction

Recent progress in nanotechnologies and plasmonics promotes the development of new types of spectrally selective nanocomponents and devices needed in non-linear optics, laser physics, optoelectronics, energy and high-density data storage, information technologies, life sciences, and security [6,20,29,36,37].

Disperse plasmonic nanostructures, that is, materials containing noble-metal nanoparticles, are highly attractive owing to their unique optical properties caused by localized surface plasmon resonances (LSPR) of light attenuation accompanied by strongly enhanced optical fields near metal nanoparticles in this spectral range. The LSPR appears upon photoexcitation in the visible and near IR regions and re-

* Corresponding author. E-mail: ponyavina@imaph.bas-net.by

M.I. Mishchenko et al. (eds.), *Polarimetric Detection, Characterization, and Remote Sensing*
DOI 10.1007/978-94-007-1636-0_15, © Springer Science+Business Media B.V. 2011

sults from collective electron oscillations confined by a metal-nanoparticle surface [7,21].

Among the most promising passive plasmonic nanomaterials are self-organized and densely packed metal–dielectric nanostructures [27,30,33] as well as layered metal–dielectric nanocomposites [3,5,24,25]. Their optical properties are further defined by collective effects resulting from the electronic and electrodynamic couplings and hence can be effectively tailored by an appropriate choice of material and nanostructure parameters.

In order to establish stable correlations between optical and topological properties of these plasmonic nanomaterials, one still needs to study and clarify the nature and manifestations of collective effects in more detail. This chapter is a brief review of results and outstanding problems in this novel field of plasmonics related to metal–dielectric nanocomposites with partially-ordered structures.

2. Localized surface plasmon resonance: spectral and near-field features

It is already well known that the fundamental difference of the optical properties of metal nanoparticles from both the properties of bulk samples and the characteristics of individual atoms is caused by resonance collective oscillations of conduction electrons near the surface of a metal particle induced by a light wave with an appropriate frequency ω_0, called the Frolich frequency, defined approximately by the following conditions:

$$\mathrm{Re}[\varepsilon(\omega_0)] = -2\,\mathrm{Re}[\varepsilon_0(\omega_0)], \quad \mathrm{Im}[\varepsilon(\omega_0)] \approx 0, \quad \mathrm{Im}[\varepsilon_0(\omega_0)] \approx 0. \tag{1}$$

Here $\varepsilon(\omega_0)$ and $\varepsilon_0(\omega_0)$ are the dielectric permittivities of the metal particle and the surrounding medium, respectively.

In the electrostatic limit, it is easily seen that these conditions maximize both the scattering (Q_{sca}) and the absorption (Q_{abs}) efficiency factor of a spherical particle:

$$Q_{\mathrm{sca}} = \frac{8k^4r^4}{3}\left|\frac{\varepsilon-\varepsilon_0}{\varepsilon+2\varepsilon_0}\right|^2, \quad Q_{\mathrm{abs}} = 4kr\,\mathrm{Im}\left[\frac{\varepsilon-\varepsilon_0}{\varepsilon+2\varepsilon_0}\right].$$

Here, k is the wave number and r is the particle radius.

LSPRs of individual metal particles defined in the visible through their extinction efficiency are highly sensitive to the nanoparticle material, size, shape, and internal structure as well as to the dielectric properties of the surrounding medium. One of the main features of an LSPR, which manifests itself as a change of color of a sparse metal colloid, is the red shift of the LSPR with increasing nanoparticle size (see Fig. 1) or increasing refractive index of the surrounding medium. This feature is caused by retardation effects and the Coulomb screening, both reducing the surface plasmon frequency [21].

It is also important to note that increasing the particle size up to tens or hundreds of nanometers also leads to drastic changes in the modal structure of the extinction spectrum of non-interacting nanoparticles, viz., higher-order modes ap-

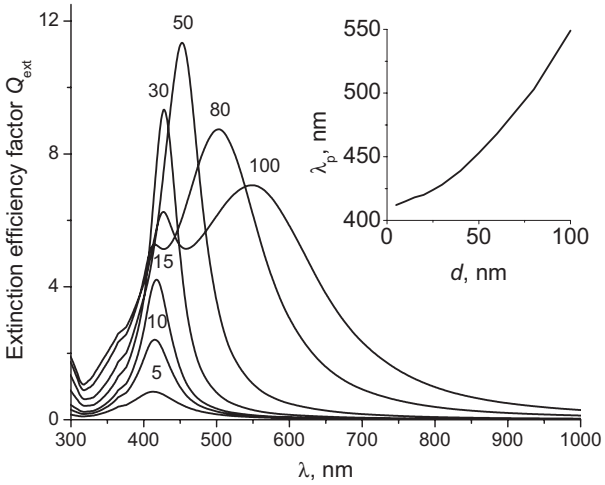

Fig. 1. Spectral extinction efficiency factors of silver nanoparticles dispersed in a medium with a refractive index of 1.5 for different particle diameters (as indicated near the respective curves). The insert shows the dependence of the LSPR peak wavelength on the particle diameter.

pear, while the modes' relative weights change. For low-order modes, the type of plasmon-excitation decay changes from non-radiative to radiative, while particles become strong scatterers. In the respective spectral regions, the SPRs in the extinction spectra of nanoparticles essentially become scattering resonances (see Fig. 2).

To calculate individual-nanosphere LSPRs, one can use the Mie theory, while other advanced single-scattering numerical techniques (such as the DDA, VIEF, and *T*-matrix methods) can be applied to nonspherical nanoparticles and nanoparticle clusters [26,32].

As a rule, experimentally measured LSPR bands are much broader than the theoretically calculated ones, even for arrays with a high degree of nanoparticle monodispersity. The nature of the strong widening of bands is still under discussion [23]. One of the main causes is the so-called internal size effect resulting in a modified nanoparticle permittivity ε. Most easily understood is the explanation of the size-dependent permittivity ε in the framework of the ballistic model, also known as the limitation of the electron mean free path (LEMFP) model [21]. An attractive feature of this approach is that it yields the size-dependent ε of metal nanospheres and nanoshells [11] in a closed analytical form.

According to the LEMFP model, the scattering of conduction electrons at the nanoparticle surface leads to a reduction in the effective mean free path of electrons compared to that in a bulk material. The longer the mean free path of electrons in the bulk material, the wider the range of nanoparticle sizes for which the internal size effect is observed. Among noble metals, this range is the widest for

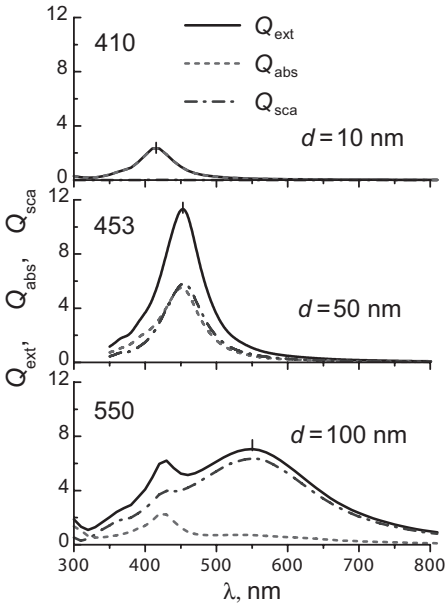

Fig. 2. Spectral dependence of extinction, absorption and scattering efficiency factors for silver nanospheres with different diameters *d*, embedded in the matrix with a refractive index of 1.5.

silver nanoparticles. Despite this factor, the LSPR of Ag nanoparticles is the most promising from the practical standpoint, owing to the ready availability of this material. Furthermore, radiative losses and high-order modes appear for silver nanoparticles at smaller sizes than for copper and gold nanoparticles. All of these traits are a consequence of the difference in the spectral interval between the LSPR and interband absorption for these noble metals.

However, the knowledge of scattering and/or absorption efficiency factors is not sufficient to define the optical spectra of densely packed plasmonic arrays which depend, via strong electrodynamic coupling, on both far-field and near-field characteristics of single scattering.

As to plasmonic nanoparticles, their near-field patterns are still poorly known in comparison with their far-field spectral and scattering counterparts. We can only mention the detailed study of the near-field enhancement ("hot spots") for fractal plasmonic nanoarrays based on the electrostatic approximation [36] and limited data on single plasmonic nanoparticles (see references in [6]) obtained with the Mie theory and the DDA technique. These data demonstrate a high sensitivity of the near-field distribution to particle sizes, shapes, and internal structures as well as to optical properties of the surrounding medium and the polarization state of the incident light. For example, it has been recognized that the maximal

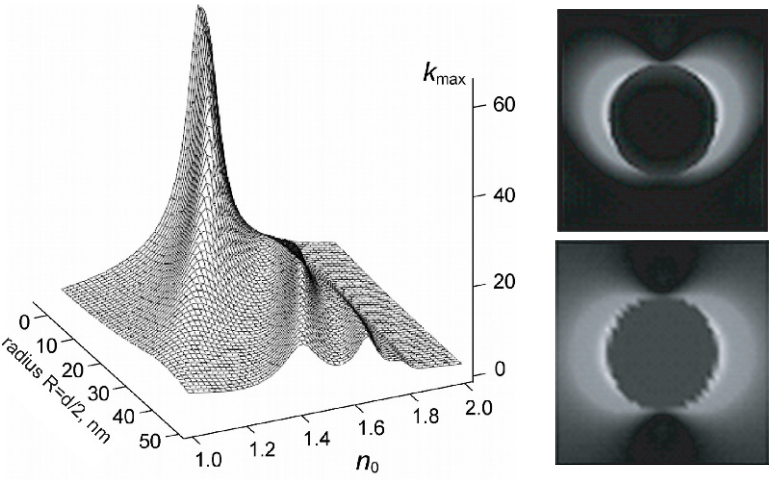

Fig. 3. On the left: dependence of the coefficient of maximal local electric field enhancement near a silver nanosphere on its size and the refractive index of the surrounding medium. On the right: near-field distributions for silver nanospheres with $d = 50$ nm (upper panel) and 20 nm (lower panel). The wavelength is 400 nm (after [2]).

coefficient of the local field enhancement for silver nanospheres exhibits a non-monotonous dependence on nanoparticle sizes and the matrix refractive index (see Fig. 3).

The most important feature essential for the understanding of the near-field contribution to electrodynamic coupling is that the hot-spot distribution strongly expands along the direction of the incident light if the particle size and/or the matrix refractive index increase [2,28].

3. Statistical approach to 2D densely packed metallic nanoparticle arrays

Electrodynamic coupling manifests itself as multiple coherent re-scattering and, as a consequence, is highly sensitive to the type of plasmonic nanoparticles and their packing density. For these reasons, the existing effective-medium theories are not always convenient and/or adequate [7]. Modeling and studies of coupled nanoarrays are considered to be one of the frontiers of modern theoretical plasmonics. In the framework of the electrostatic approximation, the features of SPRs in fractal arrays of metal nanoparticles have been studied in [36]. Two-dimensional (2D) and three-dimensional (3D) regular plasmonic nanoarrays were analyzed with the use of the plane-wave expansion method [31], the finite-difference time-domain method, and the transfer-matrix method [39]. In [38], certain principles of the theory of multiple scattering of waves were combined with the Bloch wave's formalism, which allows one to calculate both the band structure and the transmission and reflection coefficients for perfectly regular particle ar-

rays. However, topological and/or size disorders introduced in plasmonic nanomaterials during their fabrication with one of the existing technologies allows one to classify these materials as not perfectly regular, but rather as highly-ordered arrays of nanoparticles.

In our opinion, an effective way to describe the features of electrodynamic coupling in partially ordered plasmonic nanoarrays is to use the approach based on the statistical theory of multiple scattering of waves (STMSW) [9]. According to the STMSW, the resulting field $\mathbf{E}(\mathbf{r})$ at any point in space $\mathbf{r}$ (either inside or outside a disperse medium) and the effective field $\mathbf{E}_{\text{eff}}(\mathbf{r})$ at any particle are both superpositions of the incident and multiply scattered waves:

$$\begin{aligned} \mathbf{E}(\mathbf{r}) &= \mathbf{E}_0(\mathbf{r}) + \sum_j \mathbf{t}(\mathbf{r}, \mathbf{r}_j)\,\mathbf{E}_{\text{eff}}(\mathbf{r}_j), \\ \mathbf{E}_{\text{eff}}(\mathbf{r}_j) &= \mathbf{E}_0(\mathbf{r}_j) + \sum_{j \neq i} \mathbf{t}(\mathbf{r}_j, \mathbf{r}_i)\,\mathbf{E}_{\text{eff}}(\mathbf{r}_i). \end{aligned} \tag{2}$$

Here $\mathbf{t}(\mathbf{r}, \mathbf{r}_j)$ is the single-particle scattering operator.

The STMSW accounts for electrodynamic coupling in spatially correlated arrays through the superposition and subsequent averaging of fields scattered by all nanoparticles. The STMSW operates with the field moments, which are the values averaged over all possible configurations of a given particle array. The main characteristics of the STMSW are the mean (or coherent) field $\langle \mathbf{E}(\mathbf{r}) \rangle$, the coherent intensity $I_{\text{c}} = |\langle \mathbf{E}(\mathbf{r}) \rangle|^2$, and the field covariance $\langle \mathbf{E}(\mathbf{r}) \cdot \mathbf{E}^*(\mathbf{r}) \rangle$.

Lax [22] proposed to average Eqs. (2) over different configurations of a particle ensemble with the assumption that the fixation of any particle specifies the spatial configuration of the whole assembly. It is clear that the more regular the particle array, the better this assumption. This scheme was called the quasicrystalline approximation (QCA). More recently, Hong [8] considered 2D particles ensembles in the framework of the QCA and derived the following system of two equations defining the mean field at a $\mathbf{r}$:

$$\begin{aligned} \langle \mathbf{E}(\mathbf{r}) \rangle &= \mathbf{E}_0(\mathbf{r}) + p_0 \int d\mathbf{R} \int d\mathbf{r}' \boldsymbol{\Gamma}(\mathbf{r}, \mathbf{r}' + \mathbf{R}) \langle \mathbf{E}(\mathbf{r}' + \mathbf{R}) \rangle_{\mathbf{R}}, \\ \langle \mathbf{E}(\mathbf{r} + \mathbf{R}) \rangle_{\mathbf{R}} &= \mathbf{E}_0(\mathbf{r} + \mathbf{R}) + \int d\mathbf{r}' \boldsymbol{\Gamma}(\mathbf{r} + \mathbf{R}, \mathbf{r}' + \mathbf{R}) \langle \mathbf{E}(\mathbf{r}' + \mathbf{R}) \rangle_{\mathbf{R}} \\ &\quad + p_0 \int d\mathbf{R}'\, g(|\mathbf{R} - \mathbf{R}'|) \int d\mathbf{r}' \boldsymbol{\Gamma}(\mathbf{r} + \mathbf{R}, \mathbf{r}' + \mathbf{R}') \langle \mathbf{E}(\mathbf{r}' + \mathbf{R}') \rangle_{\mathbf{R},\mathbf{R}'}, \end{aligned} \tag{3}$$

where p_0 is the number of particles per unit area; $\mathbf{E}_0(\mathbf{r})$ is the incident field, $\langle \mathbf{E}(\mathbf{r}) \rangle_{\mathbf{R}}$ is the average field with one particle fixed at a point $\mathbf{R}$; $\langle \mathbf{E}(\mathbf{r}' + \mathbf{R}') \rangle_{\mathbf{R},\mathbf{R}'}$ is the average field with two particles fixed at points $\mathbf{R}$ and $\mathbf{R}'$; $\boldsymbol{\Gamma}(\mathbf{r}, \mathbf{r}')$ is the tensorial Green function; and $g(|\mathbf{R} - \mathbf{R}'|)$ is the radial distribution function defined as the probability for two particles to be separated by a distance $R = |\mathbf{R} - \mathbf{R}'|$.

Characteristic features of the radial distribution function depend on the type of disperse medium. For a sparse medium, when interparticle distances are considerably greater than the particle size, $g(|\mathbf{R} - \mathbf{R}'|) = 1$ for any $|\mathbf{R} - \mathbf{R}'| \geq d$. This

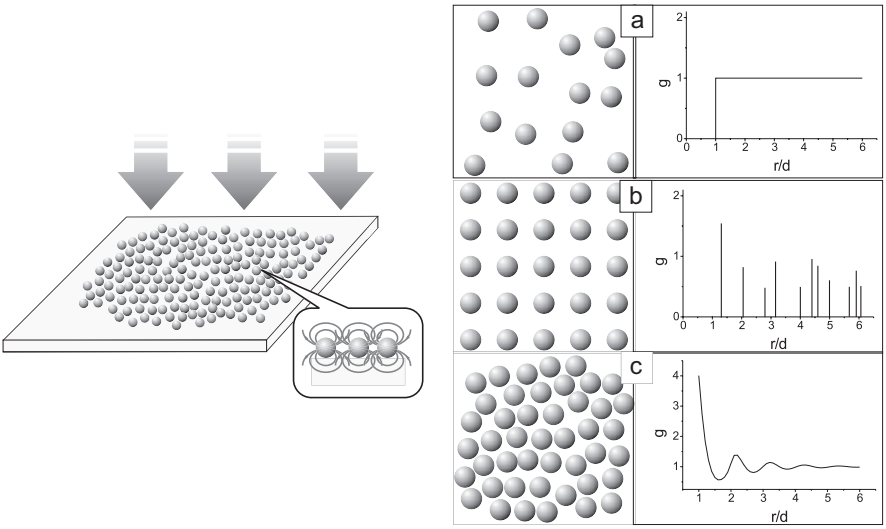

Fig. 4. The structure of a densely packed monolayer (on the left) and radial distribution functions (on the right) of (a) a sparse random as well as (b) regularly and (c) densely packed partially ordered disperse layers.

means that the particles are randomly distributed and the scattered wave phases are random. On the other hand, regular structures like "nanoparticle crystals" are characterized by long-distance ordering. Particles embedded at specific locations in the "crystal lattice" are separated by well-defined distances. For a perfect regular particle array, the $g(|\mathbf{R}-\mathbf{R}'|)$ is a set of delta functions corresponding to the fixed lattice nodes $\mathbf{R}_i$. In this case, the scattered wave phases are perfectly deterministic.

A partially ordered structure occupies an intermediate place between the extreme cases of a sparse group and a regular system. For example, as can be seen in Fig. 4, densely packed arrays are characterized by short-range ordering. The locations of neighboring particles are partially correlated due to finite particle sizes and the high particle concentration. As a consequence, $g(|\mathbf{R}-\mathbf{R}'|)$ has pronounced maxima corresponding to the most probable distances between particles. For particles located in the range of short ordering, the scattered waves are partially coherent, and the corresponding phase relations are not random. The stronger the spatial ordering owing to an increased particle concentration, the more significant the interference of the scattered waves. The denser the nanoparticle packing, the stronger the near-field coupling.

The $g(|\mathbf{R}-\mathbf{R}'|)$ function for a densely packed system of particles can be calculated by using the model of solid spheres in the framework of the Percus–Yevick approximation [42].

When the particles are spheres, it is convenient to solve Eqs. (3) by expanding the electromagnetic fields and the tensorial Green function in vector spherical harmonics. Then one obtains the following relations for the coherent transmission T_m and reflection R_m coefficients of a partially ordered monolayer of monodisperse particles [1,34,35]:

$$T_m = \left| 1 - \frac{\pi}{k^2} p_0 \sum_l (2l+1)(b_{lM} + b_{lE}) \right|^2, \qquad R_m = \left| -\frac{\pi}{k^2} p_0 \sum_l (-1)^l (2l+1)(b_{lM} - b_{lE}) \right|^2. \tag{4}$$

Here, the coefficients b_{lM} and b_{lE} are determined from the following system of equations:

$$b_{lM} = b_l + p_0 b_l \sum_{l'} (P_{ll'} b_{l'M} + Q_{ll'} b_{l'E}),$$
$$b_{lE} = a_l + p_0 a_l \sum_{l'} (P_{ll'} b_{l'M} + Q_{ll'} b_{l'E}),$$

where a_l and b_l are the Mie coefficients. The terms containing the functions $P_{ll'}$ and $Q_{ll'}$ depend on $g(|\mathbf{R} - \mathbf{R}'|)$ in a complicated manner [34]. When the individual-particle permittivity becomes size-dependent, one must take this into account while calculating the Mie coefficients.

It can easily be shown that neglecting the lateral electrodynamic coupling in Eqs. (3) yields the following simple analytical expressions for the coherent transmission and reflection coefficients:

$$T_m = 1 - \eta Q_{\text{ext}} + \frac{4\pi\eta^2}{\rho^2} x(0) \Lambda Q_{\text{ext}}, \quad R_m = \frac{4\pi\eta^2}{\rho^2} x(0) \Lambda Q_{\text{ext}}. \tag{5}$$

Here, Q_{ext}, $x(\gamma)$, and ΛQ_{ext} are the single-particle extinction efficiency factor, phase function, and scattering efficiency factor, respectively; $\rho = \pi d/\lambda$ is the size parameter; d is the particle diameter; and $\eta = p_0 \pi d^2/4$ is the monolayer overlap parameter defined as the fraction of a monolayer area occupied by nanoparticles. Note, that these expressions, called the coherent single-scattering approximation (CSSA), can be quite accurate if the single-particle phase function is strongly elongated in the forward-scattering direction.

4. Electrodynamic coupling and spectral properties of 2D densely packed plasmonic nanostructures

Surface plasmon photoexitation in nanoarrays consisting of densely packed or partially ordered metal nanoparticles has a collective nature. Small interparticle distances and short-range ordering of particles cause strong electrodynamic coupling. Its optical manifestations strongly depend on sizes of plasmonic nanoparticle.

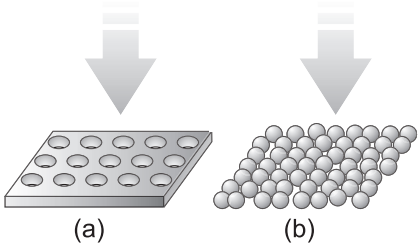

Fig. 5. Two-dimensional metal–dielectric nanostructures: (a) a perforated thin metal film and (b) a densely packed array of metal nanoparticles (after [15]).

4.1. Enhanced transmission through monolayers with extremely dense packing of submicron plasmonic nanoparticles

The recent discovery of enhanced resonant transmission of light through optically thick metal films perforated with an array of subwavelength holes [4] has attracted great attention, and its plasmon-induced origin in the case of *perforated* structures of different geometries is now actively explored. An analogous phenomenon is expected to arise in 2D densely packed *disperse* metal structures with the scale of inhomogeneities comparable to that in perforated metal films. One particular example is a 2D array of densely packed, submicrometer metal nanospheres, which is essentially the reverse of an array of holes in a metal film (compare Fig. 5b with Fig. 5a). Substantial progress in the synthesis of such 2D arrays of submicrometer metal nanoparticles by a self-assembling organization has recently been reported [20].

We analyzed theoretically the feasibility of enhanced transmission of visible light through 2D random, densely packed arrays of submicrometer noble-metal nanoparticles and established its electrodynamic nature [15].

Figure 6 shows spectra of the direct transmission of light through a 2D densely packed nanoparticle array calculated in the framework of the QCA, wherein the lateral electrodynamic coupling between particles is considered as the interference of multiply scattered waves in partially-ordered arrangement of scatterers. The transmission spectrum of an equivalent sparse system composed of non-interacting nanoparticles was calculated from the standard Bouger law: $T_B = \exp(-\eta Q_{\text{ext}})$. As one can see, the densely packed array is characterized by an enhanced long-wavelength transmission (ET) with a peak value of 87% (and even higher for larger particles) within a lower-order surface plasmon extinction band inherent to the same but uncoupled particles. Thus, the 2D disperse metal–dielectric layers of submicron silver nanoparticles can exhibit enhanced transparency in the LSPR spectral region (see also [19,27]). The ET is a result of constructive interference coupling between the incident light and radiative delocalized surface plasmon modes of lower orders. This effect becomes stronger with increasing density, since the scale of surface plasmon localization increases due to increasing range of nanoparticle correlations and near-field coupling.

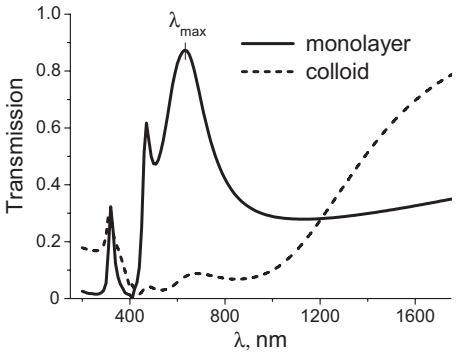

Fig. 6. Transmission spectrum of a 2D densely packed array of silver particles ($d = 200$ nm; $\eta = 0.7$; $n_m = 1.5$) and that of a sparse system consisting of the same particles (after [15]).

It should be noted that 2D disperse nanostructures have obvious advantages over perforated metal films since they provide additional possibilities for tuning their optical response. While the change in the shape of inhomogeneities and the type of arrangement is applicable to both structures considered, the inhomogeneity composition and the controlling interior structure are realized much easier with densely packed nanoparticle arrays.

4.2. Strong light quenching by monolayers of submicron plasmonic nanoparticles

With an intermediate concentration of submicrometer plasmonic particles in a monolayer, a strong resonance quenching (SRQ) may arise. The SRQ was observed experimentally for the first time by Chumanov with colleagues for monolayers consisting of 100-nm Ag nanoparticles and having an overlap parameter of 0.3 [27]. It is worthwhile to note that their experimental results are in excellent agreement with our simulations based on the QCA (see Fig. 7).

Among the reasons leading to the SRQ, specific plasmonic coupling and near-field effects have been suggested in [27]. However the fact that the most pronounced SRQ was realized not with the highest but rather with intermediate concentrations necessitates searching for other mechanisms rooted in coherent scattering.

In order to answer the question concerning the nature of this effect, let us consider the simplest scheme of multiple coherent scattering (namely the CSSA), which takes into account coherent coupling only as the interference of waves singly scattered by individual particles (see Eqs. (5)). Re-scattering between particles is not taken into account. Each individual particle is illuminated by the incident wave only. This model yields simple conditions of the total interference quenching (TIQ) caused by a destructive interference of the incident and scattered waves. This happens when the amplitudes of the incident wave and the total scattered

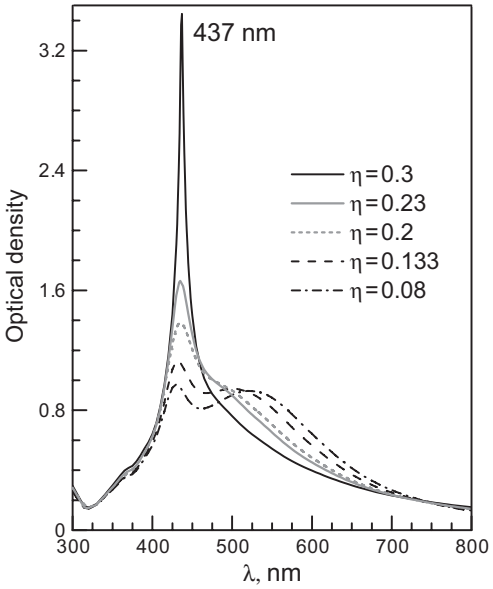

Fig. 7. Optical density of 2D arrays of $d = 100$ nm silver particles embedded in polydimethylsiloxane, for different surface particle concentrations. The calculation are based on the QCA for the experimental conditions of [27].

wave are equal, while their phases are opposite [10]. According to Eq. (5), $T_m = 0$ if

$$\frac{16\,|S(0)|^2}{\rho^4 Q_{\text{ext}}} = Q_{\text{ext}}, \quad \eta_0 = \frac{\rho^4 Q_{\text{ext}}}{8\,|S(0)|^2}.$$

Here, $S(\gamma)$ is the single-scattering amplitude.

Importantly, the conditions of the TIQ based on the CSSA are analogous to the conditions of the SRQ in the framework of the QCA. Detailed information is given in Fig. 8; as one can see, both approximations yield qualitatively similar dependences of the optimal overlap parameter and the spectral position of the SRQ on the particle size. Furthermore, for submicrometer particle sizes these results agree numerically. Residual quantitative differences are related to the fact that the CSSA does not take into account coherent re-scattering, which intensifies with decreasing size parameter.

Thus, the main results are the following. The interference quenching is never realized for monolayeres of dipole plasmonic nanoparticles, even at the highest particle concentration. The optimal overlap parameter changes non-monotonically when particle sizes grow. Furthermore, the spectral position of the SRQ gradually shifts toward the spectral position of high-order modes with increasing particle sizes.

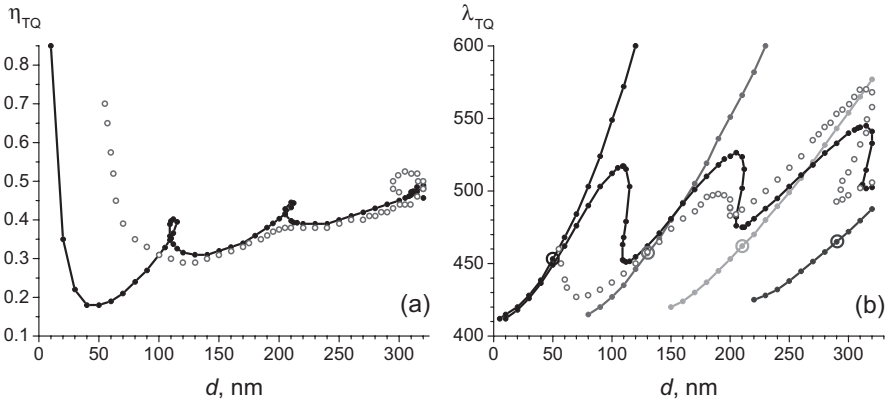

Fig. 8. (a) Optimal overlap parameter and (b) spectral position of the SRQ peak for a monolayer of silver nanoparticles embedded in a matrix with $n_m = 1.5$. Filled circles: calculations based on the CSSA (quenching until $T_m = 10^{-3} - 10^{-4}$); open circles: calculations based on the QCA ($10^{-4} - 10^{-5}$). "Branches" in (b) show spectral positions of the LSPR modes.

4.3. Concentration red shift of the collective plasmon resonance frequency

It was already noted that nanoparticle positions in the range of short ordering and the respective phases of scattered waves are strongly correlated in densely packed structures. Furthermore, for dipole nanoparticles the hot spots are concentrated in lateral directions, which supports strong near-field coupling. As a consequence, a new scale of surface plasmon localization arises. It may be quantitatively identified with the existence of "effective plasmonic particles" with a size comparable to the scale of short-range ordering. Increasing concentration leads to a growing scale of the surface plasmon localization and increasing size of the effective plasmonic particles (see Fig. 9). Thus, the close proximity and near-range ordering of dipole plasmonic nanoparticles are accompanied by the appearance of attenuation bands attributed to the coupled (collective) plasmon absorbance resonance [13,14].

It is worth noting that there are two ways of controlling the particle concentration. The first one is to adjust the system volume for a fixed number of particles (compare the solid and dot-dashed curves for $\eta = \text{const}$ in Fig. 10). The second way is to change the number of particles for the same system volume (compare, e.g., solid curves for different η in Fig. 10).

As can be seen from Fig. 10, in either case the resulting increase in the particle packing density causes a red shift of the SPR frequency calculated based on the QCA. Furthermore, when interparticle distances decrease, the enhancement of electrodynamic coupling leads to strengthening of the plasmon resonance. On the other hand, for sparse systems of the same particles (i.e., calculations based on the

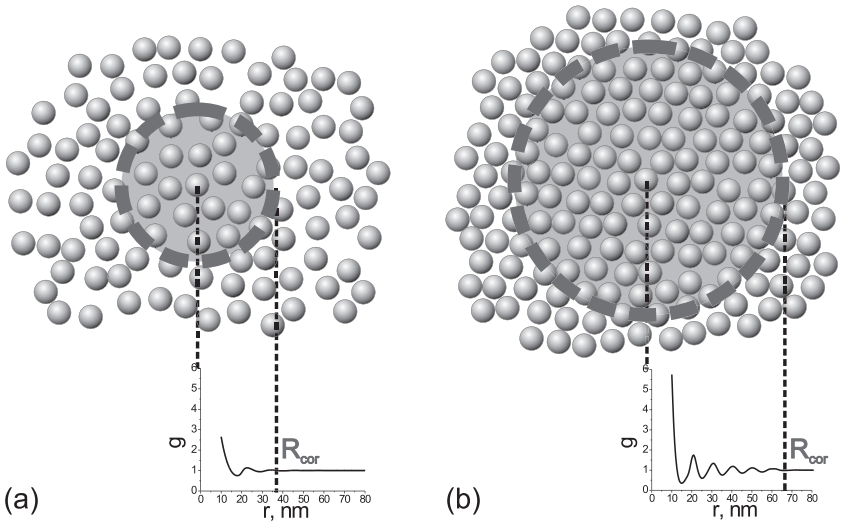

Fig. 9. Concentration-caused enlargement of the surface plasmon localization scale in 2D densely packed arrays: (a) $\eta = 0.4$ and (b) $\eta = 0.7$.

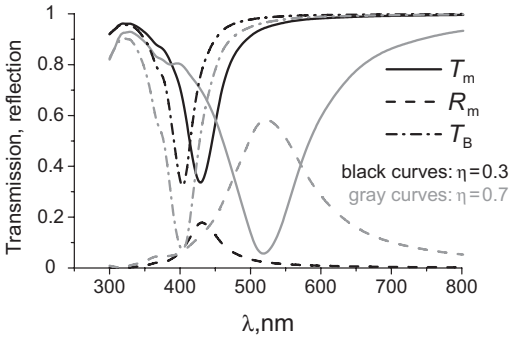

Fig. 10. Transmission T_m and reflection R_m spectra of monolayers made of silver nanospheres with $d = 2$ nm, for different overlap parameters η (the matrix refractive index $n_m = 1.4$). The transmission spectrum T_B corresponds to a sparse system of the same nanoparticles.

Bouger law), there is no plasmon frequency change with increasing overlap parameter.

The second case, wherein the particle density is modified by changing the number of particles, was realized experimentally, for example, by Kreibig et al. [21]. They noted that the interference of waves scattered by densely packed nanoparticle aggregates acts, apparently, in the same manner as the growth of an

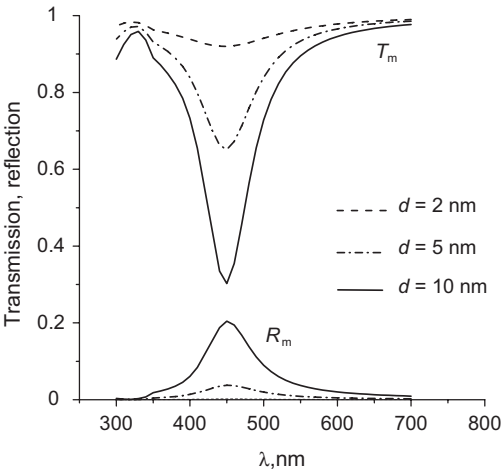

Fig. 11. Transmission T_m and reflection R_m spectra of monolayers made of silver nanospheres with different diameters d ($\eta = 0.4$ and $n_m = 1.4$).

isolated particle size. The aggregation of particles is somewhat similar to their growth. In the framework of the QCA, the appearance of densely packed nanoparticle aggregates is defined by increasing short-range ordering.

However, the red concentration shift may be caused not only by the short-range electrodynamic interactions related to the particle aggregation and, consequently, to a change in the nearest particle surrounding. In addition, it may be caused by the effective field modification as a whole when the particle concentration grows [13,14]. Apparently, a single inclusion is excited by a wave propagating in some effective medium associated with the average coherent field and characterized by the effective refractive index.

Then, by analogy with the Frolich frequency ω_0 determining the LSPR spectral position via the conditions (1), we introduce the effective Frolich frequency ω_0' which determines the collective SPR frequency:

$$\mathrm{Re}[\varepsilon(\omega_0')] = -2\,\mathrm{Re}[\varepsilon_{\mathrm{eff}}(\omega_0')], \quad \mathrm{Im}[\varepsilon(\omega_0')] \approx 0, \quad \mathrm{Im}[\varepsilon_{\mathrm{eff}}(\omega_0')] \approx 0.$$

The effect of the particle size on characteristics of the collective SPR is shown in Fig. 11. The growth of particle diameters over the considered range of Rayleigh scattering ($d < 10$ nm) is accompanied by the amplification and narrowing of the plasmon attenuation peak, with the resonance spectral position being defined only by the particle concentration.

It is interesting that selective reflectance in the SPR spectral region is enhanced significantly when the particle size increases. For example, for monolayers of silver nanoparticles with $\eta = 0.4$, the maximal reflectance increases from 5% to 20% as the particle diameter changes from 5 to 10 nm (see Fig. 11).

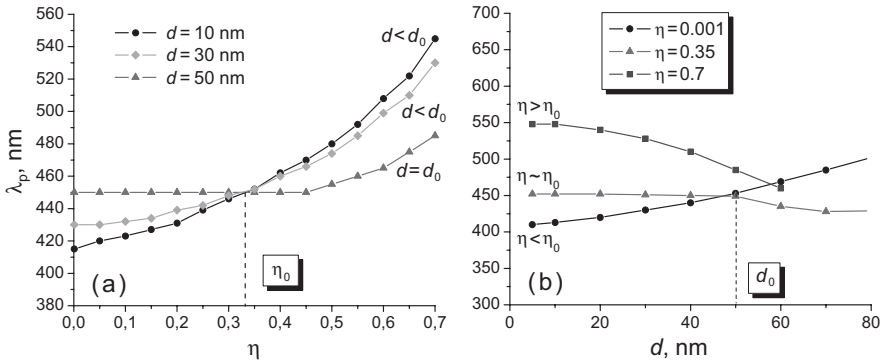

Fig. 12. (a) Concentration and (b) size dependences of the SPR peak wavelength λ_p for a silver nanoparticle monolayer [16].

Thus, the experimental data and their numerical simulation based on the QCA demonstrate that the coherent collective effects in densely packed monolayers of dipole plasmonic nanoparticles result in a red shift (with respect to that of isolated particles) of the SPR frequency as well as to the SPR amplification and broadening. The lateral electrodynamic coupling transforms the structure of plasmon resonances and effects their spectral positions.

The results on the size and concentration dependences of the dipole SPR maxima are summarized in Fig. 12. One can use these data to retrieve nanoparticle sizes and concentrations from experimental spectroscopic data [16].

4.4. Enhanced response of 2D densely packed arrays of metal nanoparticles to environmental changes

Nanostructures consisting of noble-metal nanoparticles have become increasingly popular in various sensor applications [6,36,37]. One of the most often utilized effects is the spectral shift of the SPR in response to local changes of the ambient refractive index n_m.

We analyzed theoretically the SPR spectra of 2D densely packed arrays of plasmonic nanospheres for different values of n_m, nanoparticle diameter d, and surface concentration c and revealed a dramatic growth of the sensitivity factor $S = \Delta\lambda_{\max} / \Delta n_{\max}$ with increasing η for small d (see Fig. 13) [15,41]. This growth can be explained in terms of a large effective scatterer formed by correlated nanoparticles in an array with a short-range ordering.

However, we found the largest sensitivity factors (≥ 400 nm/RIU) for 2D densely packed arrays of submicrometer noble-metal nanospheres with $d \geq 200$ nm. The spectral position of the ET band is very sensitive to changes in the surrounding medium (see Fig. 14).

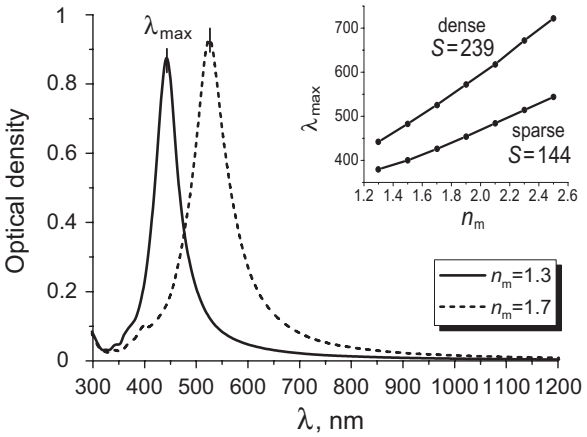

Fig. 13. Optical density spectra of a 2D densely packed array of dipole silver nanospheres (d = 10 nm, η= 0.4) in various dielectric environments. The inset shows the SPR peak position as a function of n_m for different packing densities [41].

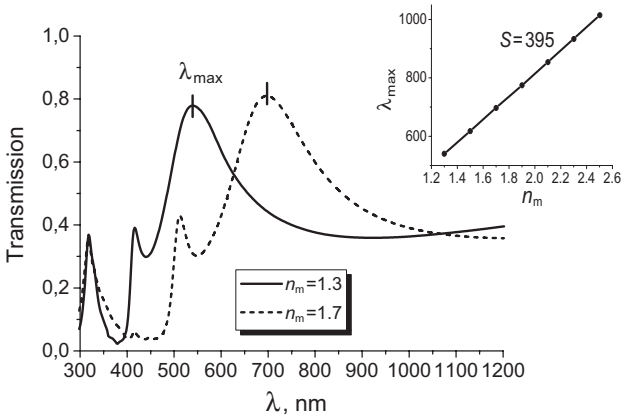

Fig. 14. Transmission spectra of a 2D densely packed array of submicrometer silver spheres (d = 200 nm, η = 0.4) in various dielectric environments. The inset shows the ET peak position as a function of n_m [15].

Figures 15 and 16 show the dependences of the SPR sensitivity on nanoparticle material and packing density. As one can see, monolayeres consisting of silver nanoparticles are much more effective than those containing gold and copper ones.

4.5. Controlling light absorption in a monolayer of metal nanoparticles

Let us now consider in more detail the spectral absorbance of densely packed monolayers of metal nanoparticles [17]. It was already noted that the maximum of

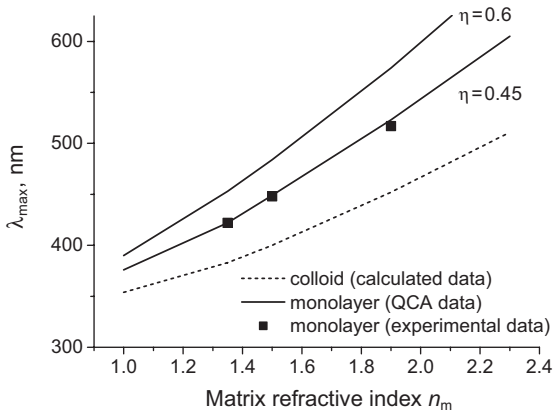

Fig. 15. Dependence of the SPR peak position on the matrix refractive index for single silver nanospheres ($d = 5$ nm) and densely packed monolayeres of such nanoparticles with different surface concentrations η (after [41]).

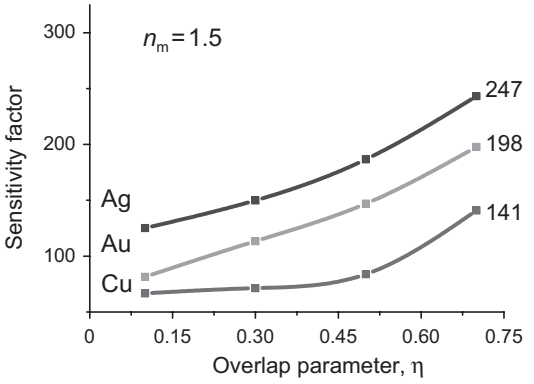

Fig. 16. Dependence of the nanoparticle monolayer sensitivity factor S on the overlap parameter for different noble metals ($d = 10$ nm; after [41]).

the absorption band is observed at the wavelength of the collective plasmon resonance λ_p. Over the Rayleigh range of particle sizes (less than 20 nm for silver), the plasmon frequency of a monolayer hardly depends on the nanoparticle diameter d and, in fact, is primarily determined by the nanoparticle surface concentration (see Fig. 17a). In contrast to λ_p, the value of maximal absorption of light at the frequency of the plasmon resonance depends strongly on the nanopartice diameter. For non-negligible surface concentrations (i.e., when the lateral electrodynamic interactions between the particles become significant), there is an optimal diameter d_0 maximizing the monolayer absorption for a given η

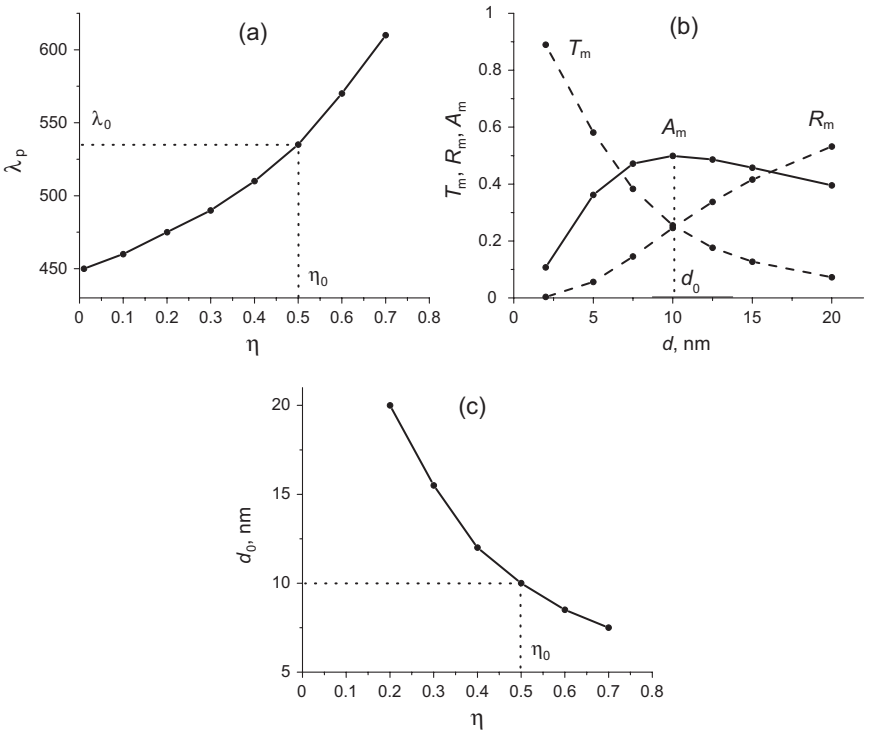

Fig. 17. Characteristics of a monolayer of silver nanoparticles in a Al_2O_3 matrix (n_m = 1.75): (a) the dependence of the plasmon resonance wavelength λ_p on the nanoparticle concentration; (b) the dependence of the resonant values of the spectral coefficients on the nanoparticle diameter for $\eta = 0.5$ ($\lambda_p = 530$ nm); (c) the dependence of the nanoparticle diameter d_0 maximizing the absorption in a monolayer on the nanoparticle concentration.

(see Fig. 17b). The dependence of d_0 on the particle concentration is shown in Fig. 17c. Since the diffuse scattering of light by a densely packed monolayer of small metal nanoparticles is negligible, the absorption of light is strictly determined by the direct transmittance, T_m, and specular reflection, R_m, coefficients: $A = 1 - T_m - R_m$.

Thus, we can propose a methodology for choosing the parameters of a monolayer that maximize the absorbance in a single monolayer of metal nanoparticles at a given wavelength.

It is interesting to note that, as follows from our numerical calculations, the maximal absorption at the plasmon frequency corresponds to the condition $T_m \approx R_m$, with T_m and R_m being equal to 25% with high accuracy. Thus, the maximal absorption in a densely packed monolayer of metal nanoparticles is equal to $A_m^{\max} \approx 50\%$. The high accuracy of these conditions in a wide range of parameters

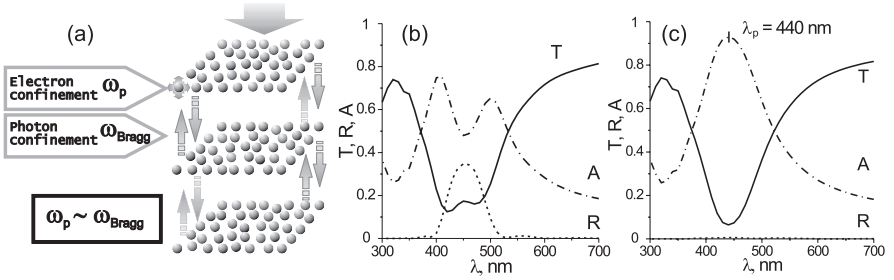

Fig. 18. (a) The general scheme and (b,c) calculated spectra of a multilayer stack composed of silver nanoparticle monolayers ($d = 3.5$ nm; $\eta = 0.4$; number of monolayers $N = 7$) separated by dielectric films with different optical thicknesses τ: (b) $\tau = \lambda_p/2$; (c) $\tau = \lambda_p/4$.

evidently implies some fundamental properties of monolayers and deserves a more detailed study.

5. Plasmonic–photonic confinement in multilayered metal nanostructures

An effective way to control spectral properties of metal nanostructures is their subwavelength periodicity leading to strong photonic confinement and causing the appearance of photonic band gaps (PBGs). Spatial ordering may be realized in different ways. Technologically, one of the simplest approaches is to form a stack of metal nanoparticle monolayers separated by solid intermediate films. A system thus formed is a kind of one-dimensional (1D) photonic crystal owing to the 1D periodicity of the dielectric function. When the PBG and the SPR are realized at similar frequencies, the photonic and plasmonic modes are strongly coupled, and the hybrid resonances are extremely sensitive to all nanocomposite parameters (see Fig. 18) [12].

The transfer matrix–QCA (TM–QCA) scheme that we used for numerical simulations defines the coherent fields transmitted and reflected by an N-monolayer stack as follows [35]:

$$\begin{aligned} \langle \mathbf{E}(\mathbf{z}) \rangle &= \exp(\mathrm{i}kz)\left(\mathbf{e} + \sum_{j=1}^{N} \mathbf{G}_j^{+} \right), \\ \langle \mathbf{E}(-\mathbf{z}) \rangle &= \exp(\mathrm{i}kz) \sum_{j=1}^{N} \mathbf{G}_j^{-} \exp[(j-1)2\mathrm{i}kl_m]. \end{aligned} \tag{6}$$

Here, $\mathrm{i} = (-1)^{1/2}$, $\mathbf{G}_j^{\pm} = \mathbf{G}(\pm\mathbf{z})$ are the scattering amplitudes in the forward and backward directions for the jth monolayer in the presence of the other monolayers of the system, and l_m is the interlayer distance, i.e., the spatial interval between the centres of adjacent monolayers.

The method of self-consistent field leads to the following system of equations:

$$\begin{aligned}\mathbf{G}_j^+ &= \mathbf{F}^+ + \mathbf{F}^+ \sum_{p=1}^{j-1} \mathbf{G}_p^+ + \sum_{p=j+1}^{N} \mathbf{G}_p^- \exp[(p-j)2\mathrm{i}kl_m], \\ \mathbf{G}_j^- &= \mathbf{F}^- + \mathbf{F}^- \sum_{p=1}^{j-1} \mathbf{G}_p^+ + \sum_{p=j+1}^{N} \mathbf{G}_p^- \exp[(p-j)2\mathrm{i}kl_m].\end{aligned} \tag{7}$$

Here, $\mathbf{F}^{\pm} = \mathbf{F}(\pm\mathbf{z})$ are the vector scattering amplitudes of the monolayer obtained in the framework of the QCA.

The sums in these equations take into account the coherent irradiation of the *j*-th monolayer by the other monolayers. Solving this set of equations with respect to $\mathbf{G}_j^{\pm}$ and substituting the result in Eqs. (6) yields the coherent fields of the multilayer structure composed of equidistant monodisperse layers.

Note that for a planar geometry, the spectral coefficients of coherent transmission and reflection can be expressed in the coherent fields as $T = |\langle \mathbf{E}(\mathbf{z}) \rangle|^2$ and $R = |\langle \mathbf{E}(-\mathbf{z}) \rangle|^2$, respectively. This approach allows one to take into account both the lateral electrodynamic coupling in each densely packed monolayer and the intermonolayer interference, i.e., the 1D photonic confinement.

Returning to Fig. 18b, for the case of intermonolayer optical distance equal to half the plasmon peak wavelength λ_p, one can see a strong and narrow reflection peak as well as a broadening and a doublet structure of the transparency spectra in the vicinity of the SPR [12,40].

The case of quarter-wavelength dielectric films (see Fig. 18c) corresponds to the PBG spectral position at the collective plasmon resonance frequency. In this case the PBG formation is accompanied by light localization in a stack, while the destructive intermediate multibeam interference minimises both the transmission and the reflection, thereby resulting in a significant absorption increase over the SPR. The absorption in a quarter-wavelength multilayer exceeds substantially the total absorption by the same number of non-interacting monolayers [40].

Thus, 1D ordering of plasmonic nanoparticle arrays allows for the tailoring of multilayer optical properties by matching the thickness of separating dielectric films to the SPR wavelength of the metal nanoparticle monolayer. The effectiveness of these manipulations based on the intermediate multibeam interference depends on the monolayer reflection and transmission spectra or, in other words, on the nanoparticle material, sizes, and surface density.

As an example, Fig. 19 shows the conditions which allow one to achieve the requisite absorption at the plasmon frequency. It is seen from Fig. 19a that like for a single monolayer (see Section 4.5), there is an optimal size of nanoparticles maximizing the quarter-wavelength-stack absorbance for a certain number and packing density of monolayers in a stack. Now, however, the optimal size of nanoparticles in a stack is determined by two factors (see Figs. 19b,c): (i) the rate of absorption saturation with increasing the number of monolayers *N* (this is determined by the fraction of light transmitted through individual monolayers, which decreases with nanoparticle sizes and surface concentrations), and (ii) by the value

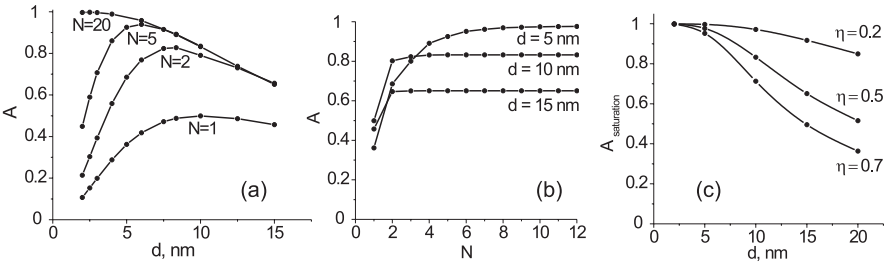

Fig. 19. Calculations for a quarter-wavelength Ag/Al_2O_3 stack. (a, b) Dependence of light absorption near the SPR frequency on (a) the diameter of silver nanoparticles in a stack of N monolayers ($\eta = 0.5$) and (b) the number of monolayers of nanoparticles with different diameters ($\eta = 0.5$). (c) Saturated absorbance as a function of particle diameter for different concentrations η.

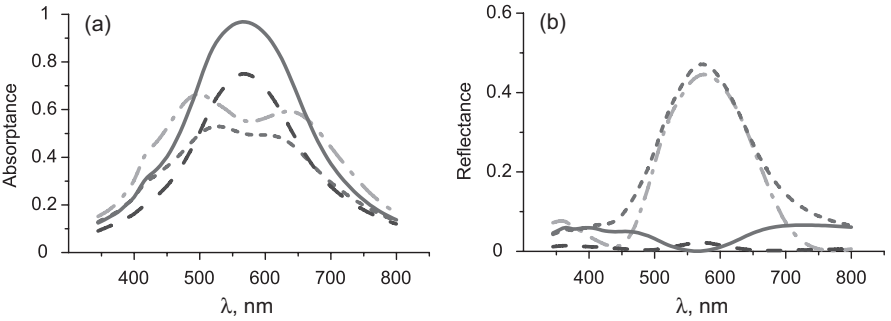

Fig. 20. Calculated (a) absorption and (b) reflection spectra for three different quarter-wavelength structures composed of two densely packed silver nanoparticle monolayers ($\eta = 0.4$). Solid curves correspond to a size-gradient system with d increasing from 5 nm to 15 nm. Dotted curves correspond to the case of the opposite-direction incidence of light on the size-gradient system. Dashed and dot-dashed curves pertain to non-gradient systems with $d = 5$ nm and $d = 15$ nm, respectively.

of the saturated absorption (which is determined by the fraction of light reflected from a monolayer and, therefore, increases with decreasing particle sizes and surface concentrations). The choice of surface concentration η is defined by the requirement of the equality of the collective plasmon resonance frequency and the frequency at which maximal absorptivity is needed.

It is worth noting that the efficiency of the destructive interference in quarter-wave systems can be enhanced by achieving comparable intensities of the beams reflected from the adjacent monolayers. To this end, in order to compensate for the increasing attenuation of light as it penetrates into a multilayer, one should maximize the reflectance of each subsequent monolayer. This can be achieved by using a gradual change of monolayer parameters [18], for example, by (i) chang-

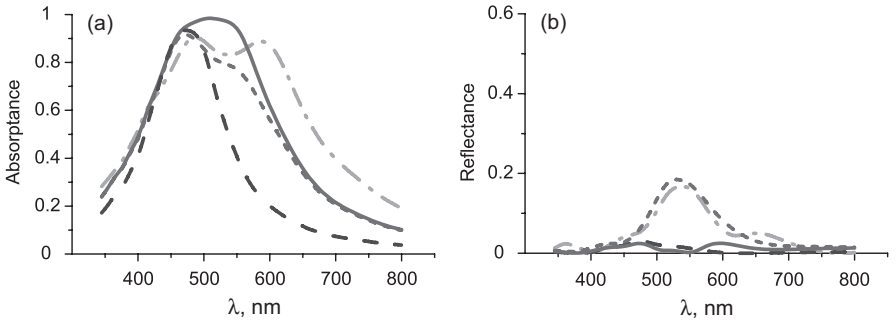

Fig. 21. Calculated (a) absorption and (b) reflection spectra for three different quarter-wavelength structures composed of five densely packed silver nanoparticle monolayers ($d = 10$ nm). Solid curves correspond to a concentration-gradient system with η increasing from 0.13 to 0.33. Dotted curves correspond to the case of the opposite-direction incidence of light on the concentration-gradient system. Dashed and dot-dashed curves pertain to non-gradient systems with $\eta = 0.13$ and $\eta = 0.33$, respectively.

ing nanoparticle sizes from monolayer to monolayer in so-called size-gradient nanostructures, and (ii) changing nanoparticle concentrations from monolayer to monolayer in so-called concentration-gradient nanostructures. For instance, in order to realize an efficient destructive interference in a quarter-wave size-gradient system, one can increase the nanoparticle size in each subsequent layer along the incidence direction.

Frequency matching of separate monolayers in a size-gradient multilayer enables one to achieve extraordinarily strong absorption with just a few monolayers in a stack (see Fig. 20). As one can see, if the incident beam first impinges on monolayer 1 then the pick absorption in this gradient two-monolayer stack is appreciably higher (97%) than for both non-gradient structures (75% and 55%). For the opposite direction of the incident beam (i.e., impinging first on monolayer 2), there is an abrupt change in the optical response (A, R) which reaches almost half the incident intensity (47%). Concentration-gradient stacks (see Fig. 21) combine the notable advantage in absorption with a negligibly small reflectance over the SPR range.

6. Conclusions

Employing spatially arranged ensembles of nanoparticles opens new ways for controlling optical properties of metallic nanostructures. Optical effects of a collective nature are dominated by different size-dependent coherent electromagnetic interactions between particles, including the near-field coupling.

Spectral manifestations of electrodynamic coupling in 2D densely packed metal–dielectric nanostructures include an enhanced long-wavelength transmission of light through a dense layer of multimode plasmonic nanoparticles; strong

resonance quenching at intermediate concentrations of submicron metal particles; and the SPR red concentration shift and enhancement of its sensitivity to the matrix refractive index in the case of dipole nanoparticles.

1D ordering of metal nanoparticle arrays combined with an appropriate choice of solid intermediate film thickness(es) gives rise to a strong photonic confinement in the vicinity of a SPR. Owing to this fact, multilayered plasmonic nanostructures enable an easy tailoring of their absorption and optical responses, which become dependent on the incidence direction for gradient-composition multilayers.

Numerical calculations based on the QCA of the STMSW along with the LEMFP model of internal size effects offer a promising way of modeling basic spectral features of 2D densely packed plasmonic nanostructures and multilayeres. The knowledge of stable spectral–structural correlations is an effective tool for initial estimation of nanoparticle materials and topological parameters ensuring desirable spectral properties of planar nanostructures. Furthermore, the strong SPR sensitivity to structural parameters of 2D densely packed metal–dielectric arrays can be used to develop improved characterization techniques based on plasmonic spectroscopy.

References

1. Bogomolov, V. N., S. V. Gaponenko, I. N. Germanenko, et al., 1997: Photonic band gap phenomenon and optical properties of artificial opals. *Phys. Rev. E* **55**, 7619–7625.
2. Dunich, R. A., and A. N. Ponyavina, 2008: Effect of metallic nanoparticle sizes on the local field near their surface. *J. Appl. Spectrosc.* **75**, 832–838.
3. Dyachenko, P. N., and Yu. V. Miklyaev, 2007: One-dimensional photonic crystal based on a nanocomposite "metal nanoparticles – dielectric". *Kompyuternaya Optika* **31**, 31–34 (in Russian).
4. Ebbesen, T. W., H. J. Lezec, H. F. Graemi, et al., 1998: Extraordinary optical transmission through sub-wavelength hole array. *Nature* **391**, 667–669.
5. Fan, Sh., P. R. Villeneuve, and J. D. Joannopoulos, 1996: Large omnidirectional band gaps in metallodielectric photonic crystals. *Phys.Rev. B* **54**, 11245–11251.
6. Gaponenko, S., 2010: *Introduction to Nanophotonics* (Cambridge University Press, Cambridge, UK).
7. Gehr, R. J., and R. W. Boyd, 1996: Optical properties of nanostructured optical materials. *Chem. Matter* **8**, 1807–1819.
8. Hong, K. M., 1980: Multiple scattering of electromagnetic waves by a crowded monolayer of spheres: application to migration imaging films. *J. Opt. Soc. Am.* **70**, 821–826.
9. Ishimaru, A., 1978: *Propagation and Scattering of Waves in Randomly Inhomogeneous Media* (Academic Press, New York).
10. Ivanov, A. P., V. A. Loiko, and V. P. Dik, 1988: *Light Propagation in Close-packed Disperse Media* (Nauka i Tekhnika, Minsk, in Russian).
11. Kachan, S. M., and A. N. Ponyavina, 2001: Resonance absorption spectra of composites containing metal coated nanoparticles. *J. Mol. Struct.* **267**, 563–564.

12. Kachan, S. M., and A. N. Ponyavina, 2002: Spectral characteristics of confined photonic and plasmonic nanostructures. *Proc. SPIE* **4705**, 88–94.
13. Kachan, S. M., and A. N. Ponyavina, 2002: Spectral properties of close-packed monolayers consisted of metal nanospheres. *J. Phys. Condens. Matter* **14**, 103–111.
14. Kachan, S. M., and A. N. Ponyavina, 2002: The spatial ordering effect on spectral properties of close-packed metallic nanoparticle monolayers. *Surf. Sci.* **507–510**, 603–608.
15. Kachan, S. M., and A. N. Ponyavina, 2007: Enhanced optical sensitivity of close-packed arrays of noble-metal nanoparticles at environmental changes. *CD International conference on Coherent and Nonlinear Optics (ICONO/LAT–2007)* (Minsk, Belarus), I02/V–6.
16. Kachan, S. M., and A. N. Ponyavina, 2007: Optical diagnostics of 2D self-assembled silver nanoparticles arrays. In V. E. Borisenko, S. V. Gaponenko, and V. S. Gurin, Eds., *Physics, Chemistry and Application of Nanostructures* (World Scientific, Singapore), pp. 165–168.
17. Kachan, S. M., and A. N. Ponyavina, 2007: Total light absorption in ultrathin size-gradient metal-dielectric nanostructures. *Proc. SPIE* **6728**, 672838.
18. Kachan, S., O. Stenzel, and A. Ponyavina, 2006: High-absorbing gradient multilayer coatings with silver nanoparticles. *Appl. Phys. B* **84**, 281–287.
19. Khlebtsov, B. N., V. A. Khanadeyev, J. Ye, et al., 2008: Coupled plasmon resonances in monolayers of metal nanoparticles and nanoshells. *Phys. Rev. B* **77**, 035440.
20. Kim, B., S. L. Tripp, and A. Wei, 2001: Self-organization of large gold nanoparticle arrays. *J. Am. Chem. Soc.* **123**, 7955–7956.
21. Kreibig, U., and M. Volmer, 1995: *Optical Properties of Metal Clusters* (Springer, Berlin).
22. Lax, M., 1952: The effective field in dense systems. *Phys. Rev.* **58**, 621–629.
23. Lerme, J., 2000: Introduction of quantum finite-size effects in the Mie's theory for a multilayered metal sphere in the dipolar approximation: application to free and matrix-embedded noble metal clusters. *Eur. Phys. J. D* **10**, 265–277.
24. Li, J., G. Sun, and C. T. Chan, 2006: Optical properties of photonic crystals composed of metal-coated spheres. *Phys. Rev. B* **73**, 075117.
25. Liao, H., W. Lu, S. Yu, et al., 2005: Optical characteristics of gold nanoparticle-doped multilayer thin film. *J. Opt. Soc. Am. B* **22**, 1923–1926.
26. Mackowski, D. W., and M. I. Mishchenko, 1996: Calculation of the *T* matrix and the scattering matrix for the ensembles of spheres. *J. Opt. Soc. Am. A* **13**, 2266–2278.
27. Malynych, S., and G. Chumanov, 2003: Light-induced coherent interactions between silver nanoparticles in two-dimensional arrays. *J. Am. Chem. Soc.* **125**, 2896–2898.
28. Messinger, B. J., K. U. von Raben, R. K. Chang, and P. W. Barber, 1981: Local fields at the surface of noble-metal microspheres. *Phys. Rev. B* **24**, 649–657.
29. Nalwa, H. S., Ed., 2001: *Nanostructured Materials and Nanotechnology* (Academic Press, New York).
30. Oraevsky, A. N., and I. E. Protsenko, 2001: Optical properties of heterogeneous media. *Quantum Electron.* **31**, 252–256.
31. Pendry, J. B., 1994: Photonic Band Structures. *J. Mod. Opt.* **41**, 209–229.
32. Penttila, A., E. Zubko, K. Lumme, et al., 2007: Comparison between discrete dipole implementations and exact techniques. *J. Quant. Spectrosc. Radiat. Transfer.* **106**, 417–436.
33. Pileni, M. P., 2001: Self-assemblies of nanocrystals: fabrication and collective properties. *Appl. Surf. Sci.* **171**, 1–14.

34. Ponyavina, A. N., and N. I. Sil'vanovich, 1994: Interference effects and spectral characteristics of multilayer scattering media. *Opt. Spektrosk*. **76**, 648–655 (in Russian).
35. Ponyavina, A. N., S. M. Kachan, and N. I. Silvanovich, 2004: Statistical theory of multiple scattering of waves applied to 3D photonic crystals. *J. Opt. Soc. Am. B* **21**, 1866–1875.
36. Shalaev, V. M., and S. Kawata, Eds., 2007: *Nanophotonics with Surface Plasmons* (Elsevier, Amsterdam).
37. Shipway, A. N., E. Katz, and I. Willner, 2000: Nanoparticle arrays on surfaces for electronic, optical and sensoric applications. *Chem*. *Phys*. *Chem*. **1**, 18–52.
38. Stefanou, N., G. Gantzounis, and C. Tserkezis, 2009: Multiple-scattering calculations for plasmonic nanostructures. *Int. J. Nanotechnol*. **6**, 137–163.
39. Wang, Z., C. T. Chan, W. Zhang, et al., 2001: Three-dimensional self-assembly of metal nanoparticles: possible photonic crystal with a complete gap below the plasma frequency. *Phys. Rev*. *B* **64**, 113108.
40. Zamkovets, A. D., S. M. Kachan, A. N. Ponyavina, and N. I. Silvanovich, 2003: Optical spectra of metal-dielectric nanocomposites with a layered subwave structure. *J. Appl. Spectrosc.* **70**, 593–598.
41. Zamkovets, A. D., S. M. Kachan, and A. N. Ponyavina, 2008: Concentration-related enhancement of the sensitivity of surface plasmon resonance of metallic nanoparticles to the characteristics of a dielectric environment. *J. Appl. Spectrosc.* **75**, 588–592.
42. Ziman, J., 1979: *Models of Disorder* (Cambridge University Press, Cambridge, UK).

Nikolai Voshchinnikov and Alina Ponyavina.

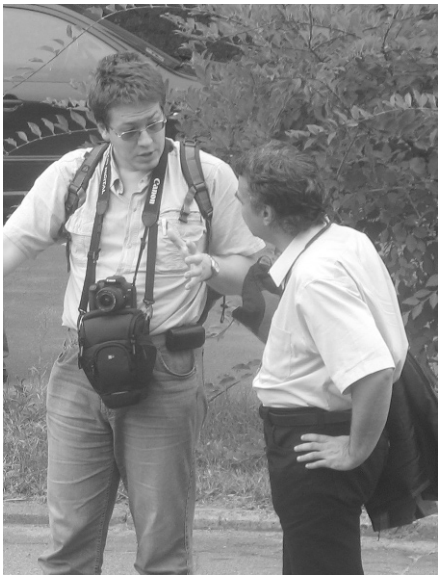

Maxim Yurkin (left) and Adrian Doicu.

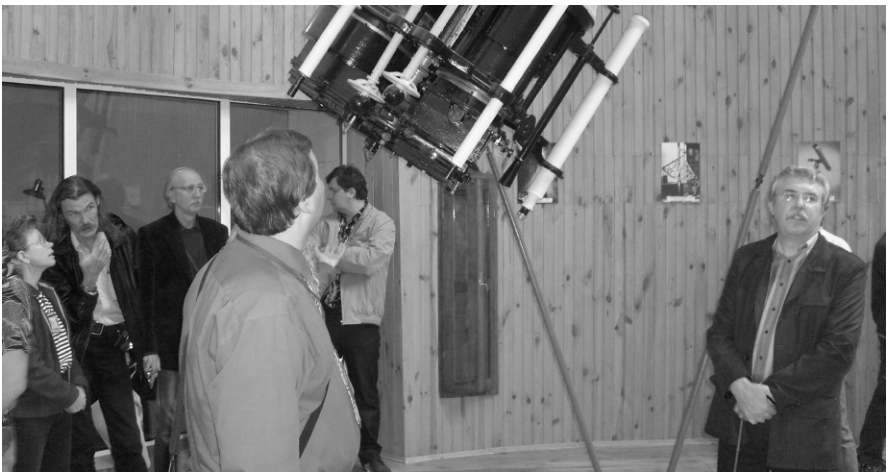

At the Museum of the Main Astronomical Observatory.

From left to right: Godern Videen, Karri Muinonen, and Klim Churyumov.

Carl Codan and Larissa Nazarenko enjoying a coffee break.